TISSUE BLOCK MRI FOR SLICE ORIENTATION-INDEPENDENT REGISTRATION OF DIGITAL HISTOLOGY IMAGES TO *EX VIVO* MRI OF THE PROSTATE

Eli Gibson[1], Cathie Crukley[5], José A. Gómez[3], Madeleine Moussa[3], Glenn Bauman[4], Aaron Fenster[125], Aaron D. Ward[1]
[1] Robarts Research Institute, [2] Department of Medical Biophysics, [3] Department of Pathology, [4] Department of Oncology, The University of Western Ontario; [5] Lawson Health Research Institute, London, Ontario, Canada

ABSTRACT

We present a method for the registration of whole-mount digital histology images to *ex vivo* MR images of the prostate that relaxes the requirement for control over specimen slicing orientation. The approach uses extrinsic fiducials visible on histology and MRI, as well as block MR images of tissue slices after coarse sectioning, to support a two-stage registration approach: (1) registration of digital histology images to block MR images, and (2) registration of block MR images to whole-specimen *ex vivo* MR images. This work presents a preliminary quantitative validation on 4 clinical prostate specimens, yielding target registration errors of 0.6 mm and 0.5 mm, respectively, for the registration stages, measured using intrinsic fiducials.

Index Terms: histopathology,imaging,registration,prostate

1. INTRODUCTION

The early diagnosis of prostate cancer increases the number of suitable treatment options and improves survival rates [1]. However, prostate cancer is currently over-diagnosed [2], potentially leading to unnecessary patient anxiety, and diagnostic and therapeutic interventions. Knowledge of the stages and grades of cancer foci within the prostate permits a reliable determination of clinical outcome[3, 4], motivating appropriate therapy selection and potentially guiding focal therapy. Accurately determining stage and grade based on biopsy material is challenging [5, 6] due to limited spatial sampling and the tendency of prostate cancer to be small and multifocal. An accurate determination of stage and grade based on 3D in vivo imaging could support more accurate diagnosis, biopsy needle guidance, and personalized therapy selection and treatment. There is evidence that correlates of stage and grade are measurable on multimodality in vivo imaging [7], but validation ideally requires the registration of these images to staged and graded histology images.

This work is part of an investigation into the utility of fused, multi-modality in vivo prostate imaging for the prediction of prostate cancer stage and grade as defined on whole-mount digital histology. *An important component of this investigation, and the focus of this paper, is the validated registration of gold standard histology images to ex vivo prostate specimen MR images.*

The problem of registration of digital histology images to *ex vivo* specimen MR images is of interest to many research groups and has resulted in the development of several techniques that facilitate this registration via a controlled physical slicing of the surgically resected prostate. Standard manual coarse sectioning of the specimen (at multi-millimeter intervals) into tissue slices is replaced with mechanical/image guidance of coarse sectioning to establish an approximate spatial relationship between the tissue slices and imaging. A recent survey [8] provides an overview of current methods. These approaches use various types of guidance to orient the cutting plane, and accuracy generally depends on the manual dexterity of a skilled operator.

Our approach reconstructs the relationship of the specimen cuts to the *ex vivo* imaging retrospectively, allowing more freedom in the cutting process. Our method is based on the observation that by taking MR images of the tissue blocks after coarse sectioning (henceforth referred to as *block MR images*), image registration techniques can be used to virtually reassemble the cut tissue blocks in a repeatable fashion. This relaxes the requirement for precise control over slicing orientation, making our technique more suitable to a clinical pathology environment.

2. MATERIALS AND METHODS

2.1 Materials

This study was conducted with the approval of the Human Subjects Research Ethics Board of The University of Western Ontario. Our ongoing study is collecting images from a total of 66 subjects undergoing radical prostatectomy. A preliminary validation of this method, based on four subjects, with three tissue slices per subject, is presented here. Specimen MR images were acquired using an endorectal receive coil with the tissue immersed in Christo-Lube (Lubrication Technology, USA) to provide a black background and minimize boundary artefacts. A T1 weighted protocol was used, with imaging parameters as follows: 3D SPGR, TR 6.5 ms, TE 2.5 ms, bandwidth ±31.25 kHz, 8 averages, FOV 14 cm, slice thickness 0.4 mm, 256×192 matrix, 160 slices, flip angle 15 degrees. Histology slides were digitized in color on a ScanScope GL (Aperio Technologies, Vista, CA, USA) bright field slide scanning system with a 0.5 μm isotropic resolution.

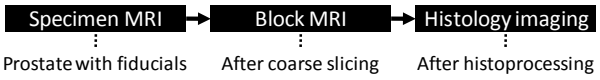

Fig. 1: Method overview. The black boxes depict imaging steps, and the solid black arrows depict the two stages of image registration performed in this work.

2.2 Methods

Our overall process is described in Fig. 1. Fiducial markers (Sec 2.2.1) were applied to the specimen prior to MR imaging. After the removal of the apex, the specimen was embedded in agar and coarsely sectioned from apex to base into 4.4 mm thick tissue blocks using a GC-9 slicer (Globe Food Equipment, Inc., Dayton, OH, USA). Block MR imaging was then performed; each block was placed into a tissue cassette and the cassettes were strapped together and imaged as a unit. Following standard histoprocessing, the tissue blocks were then paraffin embedded as whole-mounts, 4 µm-thick sections were taken from the surface of each block using a microtome, stained with hematoxylin and eosin, mounted on microscope slides, and digitized. Our clinical pathology laboratory applied consistent handling and processing schedules with timings that accommodate the size of whole mount specimens, yielding histology sections with little deformation and few artefacts or tears. Using landmark-based methods and the fiducial markers, the histology images were registered to the block MR images (Sec 2.2.2), which were then registered to the whole-specimen images (Sec 2.2.3), transitively registering the histology images to the whole-specimen MR images.

2.2.1 Fiducial marking

After 48 hours of formalin fixation, two sets of fiducials were added to each specimen: internal fiducials passing through the prostate, and external fiducials attached to the prostate surface. Fiducials were chosen to be non-disruptive to pathologists' assessments and visible on T1-weighted MRI and on histology; they are described in detail in previous work [9]. The fiducials were arranged in a consistent pattern in the apex-base (approx. inferior-superior) direction for all subjects, with 3 parallel internal fiducials and 7 external fiducials (Fig. 2). An external double fiducial was applied on the left anterior side as an orientation marker. The remaining external fiducials were arranged such that each neighboring pair formed an approximate 45 degree angle; this layout supports the determination of the inferior-superior position of any slice based on the locations of the fiducial cross sections.

2.2.2 Histology to block MR image registration

To register digital histology images to block MR images, we used a landmark-based approach, illustrated in Fig. 2A. For each extrinsic fiducial marker, enumerated as $i \in \mathbb{Z}, 1 \leq i \leq 10$, the 2D point $\boldsymbol{h}_i$ given by the fiducial cross section on a histology image corresponds to a point $m_i(s_i \in [0,1])$ along the parametric space curve defined by the fiducial on the block MR image. This correspondence was encoded by a vector of curve parameters $\boldsymbol{s} = [s_1, s_2, \cdots, s_{10}]$. Each

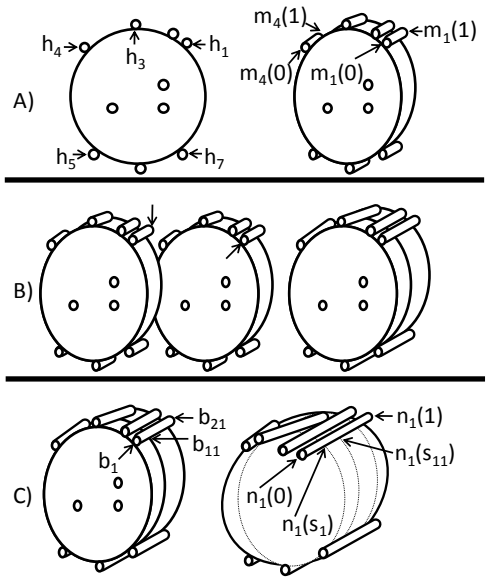

Fig. 2: Registration steps: A) Histology to block MR registration aligns fiducial point h_1 to the corresponding fiducial track m_1. B) Virtual reassembly aligns fiducial endpoints (e.g., those marked with arrows) on adjacent faces of adjacent blocks. C) Assembly to whole-specimen registration aligns assembly points b_1, b_{11}, b_{21} to the corresponding fiducial track n_1.

candidate correspondence $\boldsymbol{s}$ determines a least squares best-fit 3D affine transform $A_{\boldsymbol{s}}$ between all $\boldsymbol{h}_i$ and $m_i(s_i)$. A search of the space of correspondence vectors $\boldsymbol{s}$ finds that which yields the transformation $A_{\boldsymbol{s}}$ with the smallest residual. Because an exhaustive search of this 10D space is computationally prohibitive, we chose a triplet of fiducials corresponding to three dimensions of $\boldsymbol{s}$. We exhaustively searched this reduced 3D space of correspondence vectors $\hat{\boldsymbol{s}}$, each of which defined an affine transformation $A_{\hat{\boldsymbol{s}}}$ based on the correspondence of the chosen fiducial triplet. The residual of $A_{\hat{\boldsymbol{s}}}$ was computed using all ten fiducials, with 3D closest point correspondence used for the remaining seven fiducials. The triplet comprised three widely spaced fiducials that were entirely visible on both images and included at least one diagonal fiducial ($\boldsymbol{h}_3, \boldsymbol{h}_5$ *or* $\boldsymbol{h}_7$ in Fig. 2A).

The chosen correspondence was used to define landmark-based rigid, similarity, affine, and thin-plate spline (TPS) registrations. We evaluated each registration by computing the target registration error (TRE) as the post-registration distance between homologous intrinsic fiducials (Fig. 3) identified manually on the histology and block MR images. The selected intrinsic fiducials included ducts and corpora amylaceae less than 1 mm in diameter. 85 fiducials were identified in 12 histology images from 4 specimens.

2.2.3 Block MR to whole-specimen MR image registration

The registration of block MR imaging to whole-specimen imaging has two steps: the virtual reassembly of the prostate via the co-registration of the MR images of the individual

tissue blocks, and the registration of the reassembled prostate to the whole-specimen MRI.

In the first step, the block MR images were co-registered via the rigid alignment of the adjacent block faces of each neighboring pair of blocks. The cross sections of the extrinsic fiducial markers on each pair of adjacent block faces defined a set of corresponding landmarks (e.g., those marked with arrows in Fig. 2B), determining a rigid transformation aligning this pair of block faces. The rigid transformations for all of the pairs of block faces were composed to align all of the MR images of the individual tissue blocks, fully reassembling the prostate.

In the second step, we used a landmark-based approach, which is distinguished from that in Section 2.2.2 by the definition of the points and the parametric space curves, and by the use of a rigid transform class. This is illustrated in Fig 2C. Here, the points $\boldsymbol{b}_k$, $k \in \mathbb{Z}, 1 \leq k \leq 40$, are defined by the intersections between the 10 fiducials and the 4 cutting planes and the parametric space curves $n_i(s_k \in [0,1])$ are defined by the fiducial tracks along the entire whole-specimen MR image. This correspondence is encoded by a (4x10)-dimensional vector of curve parameters $\boldsymbol{s} = [s_1, s_2, \cdots, s_{40}]$. Each candidate correspondence $\boldsymbol{s}$ determines a least squares best-fit 3D rigid transform $R_{\boldsymbol{s}}$ between all $\boldsymbol{b}_k$ and $n_i(s_k)$. A search of the space of correspondence vectors $\boldsymbol{s}$ finds that which yields the transformation $R_{\boldsymbol{s}}$ with the smallest residual. Because an exhaustive search of this 40D space is computationally prohibitive, we chose a triplet of points corresponding to three dimensions of $\boldsymbol{s}$. We exhaustively searched this reduced 3D space of correspondence vectors $\hat{\boldsymbol{s}}$, each of which defined a rigid transformation $R_{\hat{\boldsymbol{s}}}$ based on the correspondence of the chosen fiducial triplet. The residual of $R_{\hat{\boldsymbol{s}}}$ was computed using all ten fiducials, using 3D closest point correspondence.

The chosen correspondence was used to define landmark-based rigid, similarity, affine, and TPS registrations. We evaluated the performance of each by computing the TRE using intrinsic fiducials (Fig. 3) consisting of small hypointensities and hyperintensities whose homologies were identified based on spatial relationships to other image features. 115 fiducials were identified in 12 tissue blocks from 4 specimens.

2.2.4 Block MR imaging

By imaging the coarsely sectioned tissue blocks, we establish an intermediate registration target that captures the internal anatomic structure of the prostate. While identifying intrinsic fiducials between whole-specimen MR images and histology is challenging [10], the contrast between prostate tissue and the low signal medium reveals details of internal ducts, permitting the use of intrinsic fiducial markers for the quantitative 3D validation of registrations involving this intermediate target. While the cutting of section blocks is part of standard clinical practice, this method does require an additional MR imaging session.

2.2.5 Fiducial localization

The fiducial tracks were manually located on the whole-specimen MR and block MR images at approximately 1 mm intervals centered along each fiducial track, and then interpolated to ~0.2 mm intervals using cubic splines. Fiducials on MRI were localized using a 3-plane view in 3D Slicer (Surgical Planning Lab, Harvard Medical School, Boston, USA). Fiducials on histology were localized on a 1-plane view in 3D Slicer.

Transformation	Histology-Block TRE (mm)	Block-Specimen TRE (mm)
Rigid	1.4	0.5
Similarity	0.6	0.5
Affine	0.6	0.5
TPS	0.6	0.5

Table 1: RMS TREs for the tested registration methods.

3. RESULTS

The registration of digital histology to block MR imaging and whole-specimen imaging is illustrated in Fig. 3; notice the concordance of the contents of corresponding grid cells. Table 1 gives the root-mean-squared (RMS) TRE values for the tested registrations. For the histology-block registration, transformations more flexible than a similarity transformation yield no additional accuracy, and for the

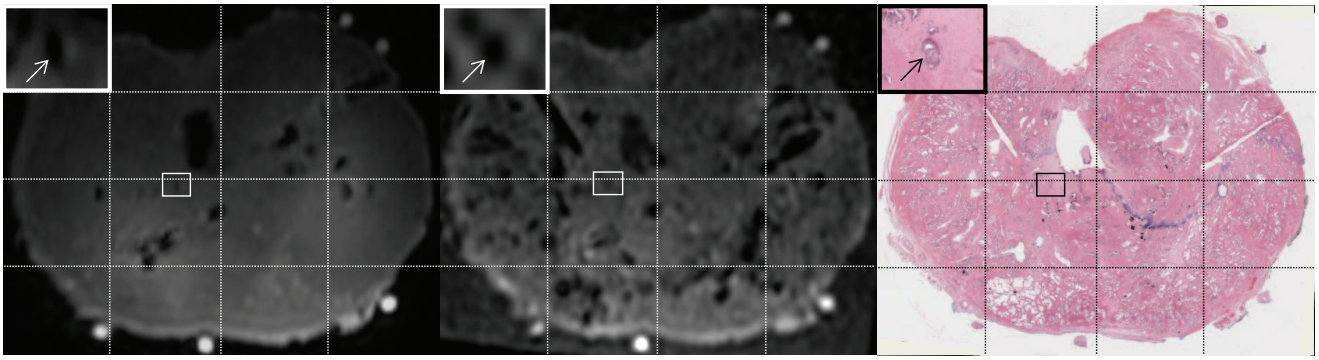

Fig. 3: Registered cross-sections from whole-specimen MRI (Left), block MRI (middle) and histology (right). Small boxed regions contain examples of the intrinsic fiducials for registration validation, and are zoomed in the top left of each image.

block-specimen registration, the same is true for rigid registration.

4. DISCUSSION

We observe in Table 1 that for the histology-block registration, the similarity transformation yields a reduced TRE, compared to that given by the rigid transformation. Since the blocks are imaged after formalin fixation, this result reflects the fact that paraffin histoprocessing causes uniform tissue shrinkage [11]. It is of interest that the affine and TPS transformations did not yield further error reductions; this suggests that histoprocessing did not cause tissue shearing or warping. Table 1 indicates that rigid registration is sufficient for block-specimen registration, suggesting minimal tissue warping after coarse sectioning, under the assumption that the fiducial localization error, which is being measured as part of ongoing work, does not dominate the TRE.

The TRE of the composition of both registrations (similarity transform for histology-block, and rigid for block-specimen) can be estimated by noting that if the errors were perfectly correlated, they would add, yielding an overall TRE of 1.1 mm, and if they were independent, then they would add in quadrature, yielding a TRE of 0.8 mm.

While several current methods for imaging-histology registration utilize whole-specimen *ex vivo* MR images, this work introduces the use of 3D volumetric block MR imaging as an intermediate registration target. In addition to enabling validation with point fiducials, it also enables correcting for variability in the spatial relationship between each 4 μm thick histology slice and the face of the 4.4 mm thick tissue block from which it is cut on the microtome. The standard practice is for the histology technologist to set the angle of the tissue block relative to the microtome blade by eye, and then remove a variable amount (from a few μm to a millimeter or more) of tissue from the front of the block face before obtaining a usable histology slice for digitization. 2D photography of the tissue block face, both prior to [12, 13] and after [10, 14, 15] microtome cutting does not capture information about this cutting angle and depth, leading to arguably strong assumptions about these parameters. Block MR imaging captures the non-parallel layout of our strand-shaped fiducial markers (Sec. 2.2.1) in 3D, permitting the accurate registration to the histology images independent of operator variability during microtome cutting (Table 1).

In finding histology to block correspondences, we avoid an exhaustive search of the ND correspondence space. Because the triplet's fiducials are visible on histology, all possible planes of cutting must pass through some point along each of the 3 fiducial tracks. Thus, an exhaustive search of the 3D correspondence space provides a wider exploration of the possible cutting planes, compared to an non-exhaustive search of the ND correspondence space using an optimizer, such as gradient descent, which may converge to the nearest local optimum.

In this work, we have presented and validated a method for the registration of *ex vivo* prostate MR images to histology images that relaxes constraints on the position and orientation of coarse specimen sectioning. The approach uses landmark-based registration of non-disruptive extrinsic fiducial markers; in contrast to image-based registration methods, our method is independent of the initial spatial alignment of the images, and blind to the intrinsic fiducials used for validation.

Acknowledgements: This work was supported by the Canadian Institutes of Health Research [CTP 87515].

5. REFERENCES

[1] M LaSpina, et al., *Update on the diagnosis and management of prostate cancer*. Can J Urol, 2008. 15 Suppl 1(3-13.

[2] HG Welch, et al., *Overdiagnosis in cancer*. J Natl Cancer Inst, 2010. 102(9): 605-13.

[3] JI Epstein, et al., *Prediction of progression following radical prostatectomy. A multivariate analysis of 721 men with long-term follow-up*. Am J Surg Pathol, 1996. 20(3): 286-92.

[4] SM Falzarano, et al., *Staging prostate cancer and its relationship to prognosis*. Diagnostic Histopathology, 2010. 16(9): 432-438.

[5] PA Humphrey, *Gleason grading and prognostic factors in carcinoma of the prostate*. Mod Pathol, 2004. 17(3): 292-306.

[6] KR Moreira Leite, et al., *Upgrading the Gleason score in extended prostate biopsy: implications for treatment choice*. Int J Radiat Oncol Biol Phys, 2009. 73(2): 353-6.

[7] HU Ahmed, et al., *Is it time to consider a role for MRI before prostate biopsy?* Nat Rev Clin Oncol, 2009. 6(4): 197-206.

[8] LH Chen, et al., *Optimum slicing of radical prostatectomy specimens for correlation between histopathology and medical images*. Int J Comput Assist Radiol Surg, 2010. 5(5): 471-87.

[9] A Ward, et al., *Registration of in vivo prostate magnetic resonance images to digital histopathology images*, *MICCAI Prostate Cancer Workshop*, 2010. 66-76.

[10] H Park, et al., *Registration methodology for histological sections and in vivo imaging of human prostate*. Acad Radiol, 2008. 15(8): 1027-39.

[11] AR Schned, et al., *Tissue-shrinkage correction factor in the calculation of prostate cancer volume*. Am J Surg Pathol, 1996. 20(12): 1501-6.

[12] G Groenendaal, et al., *Validation of functional imaging with pathology for tumor delineation in the prostate*. Radiother Oncol, 2010. 94(2): 145-50.

[13] AS Jackson, et al., *Dynamic contrast-enhanced MRI for prostate cancer localization*. Br J Radiol, 2009. 82(974): 148-56.

[14] E Bardinet, Ourselin, S., Dormont, D., Malandain, G., Tandé, D., Parain, K., Ayache, N., Yelnik, J., *Co-registration of histological, optical and MR data of the human brain.*, *MICCAI* 2002. 548-555.

[15] J Dauguet, et al., *Three-dimensional reconstruction of stained histological slices and 3D non-linear registration with in-vivo MRI for whole baboon brain*. J Neurosci Methods, 2007. 164(1): 191-204.